Supplement of Atmos. Chem. Phys., 26, 12049–12066, 2026
https://doi.org/10.5194/acp-26-12049-2026-supplement

Atmospheric Chemistry and Physics
Open Access
EGU

Supplement of

Do GEMS geostationary satellite observations of tropospheric NO_2 always improve NO_x emission estimates and related air quality modelling?

Fei Yao et al.

Correspondence to: Fei Yao (fei.yao@sjtu.edu.cn) and Paul I. Palmer (paul.palmer@ed.ac.uk)

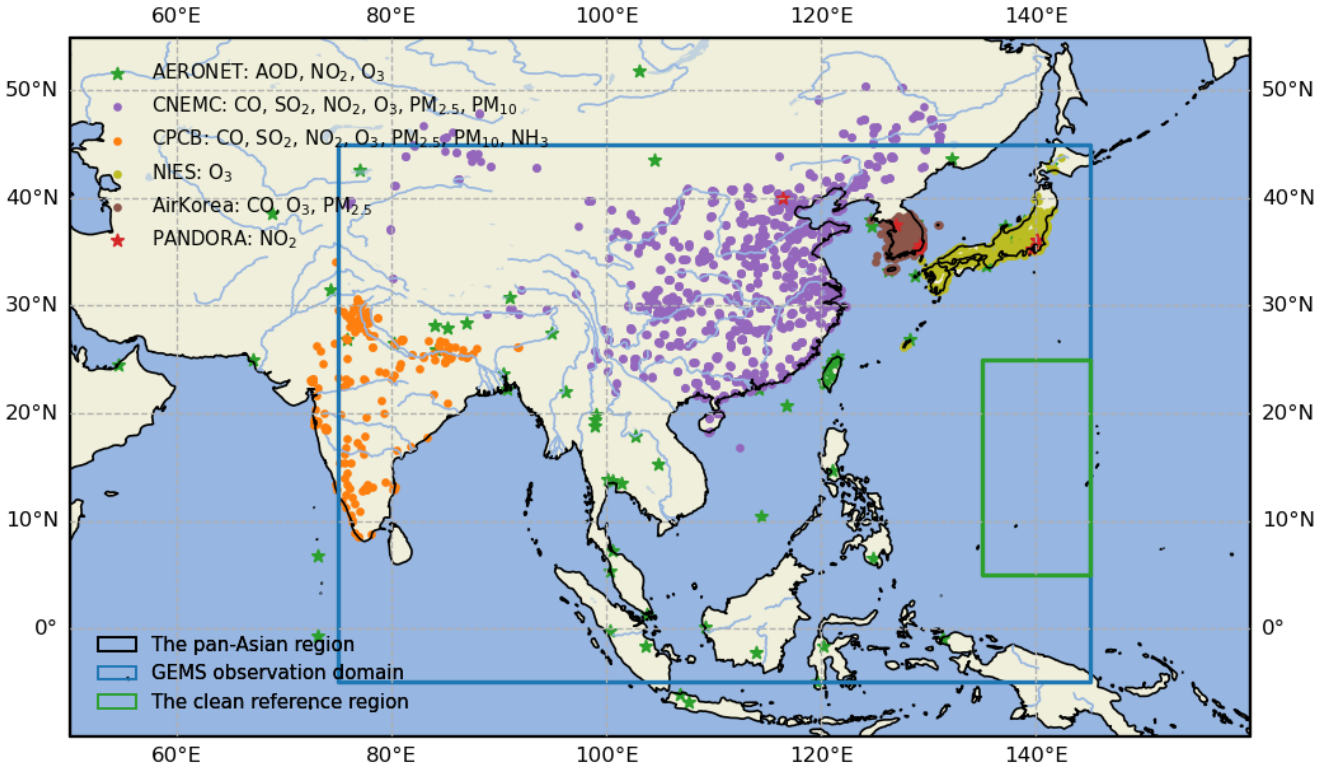

Figure S1. Geographical distributions of the multi–source *in situ* measurements used for independent model evaluation. Also shown are the pan–Asian region, GEMS observation domain, and clean reference region for defining the observation uncertainty of GEMS tropospheric NO_2 retrievals.

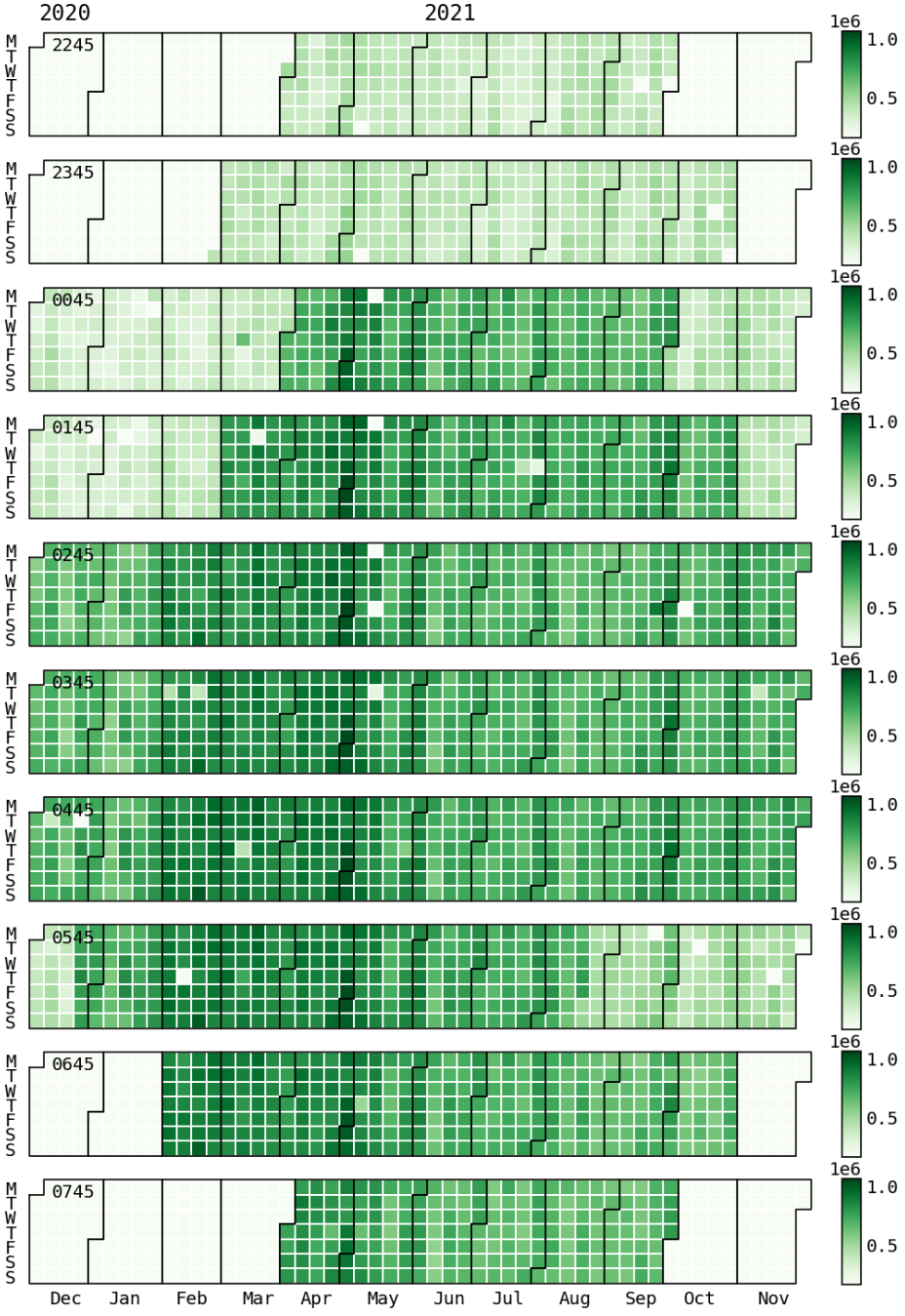

Figure S2. Hourly distributions of GEMS tropospheric NO_2 retrievals counts for all observations over the pan–Asian region.

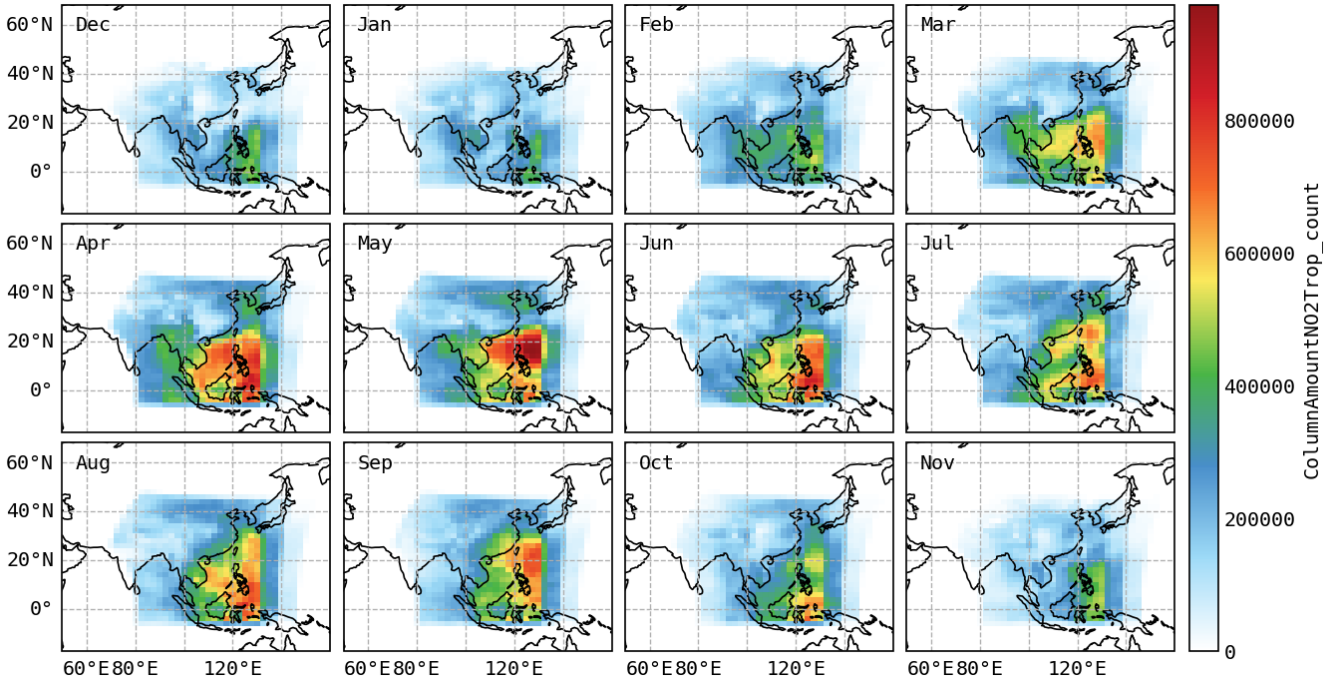

Figure S3. Geographical distributions of monthly counts of GEMS tropospheric NO_2 retrievals for all daytime observations.

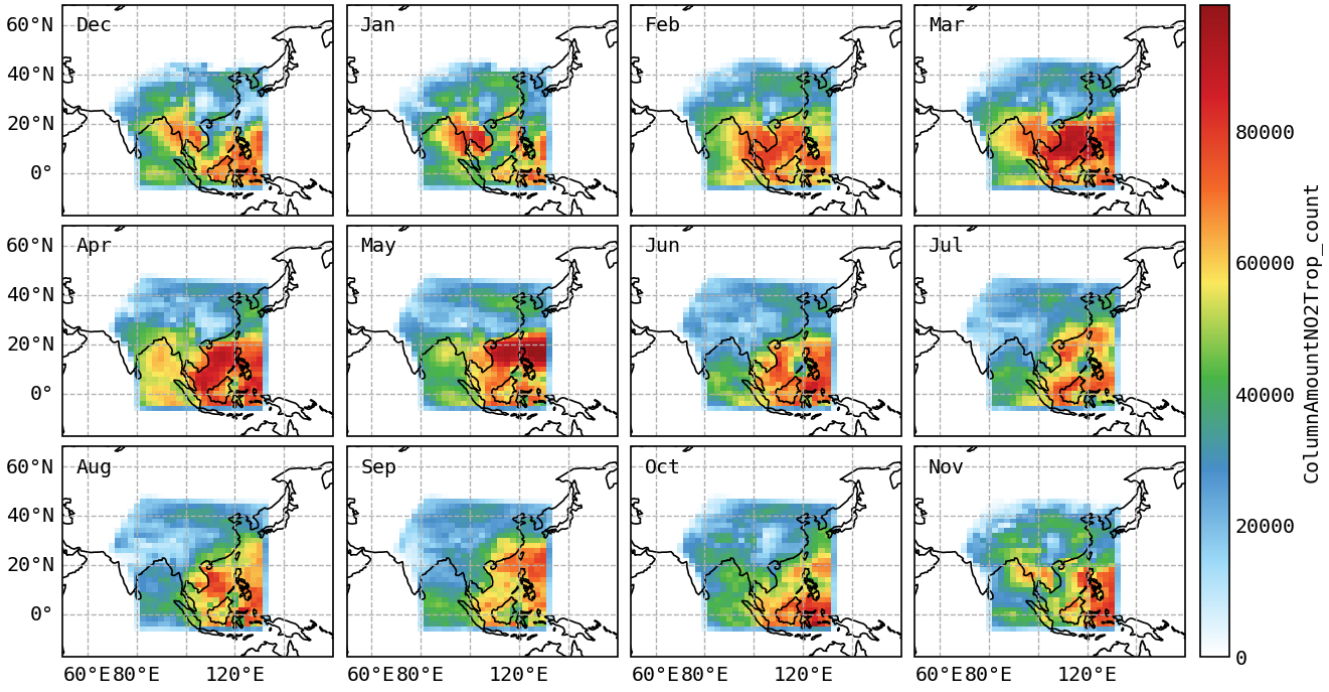

Figure S4. Geographical distributions of monthly counts of GEMS tropospheric NO_2 retrievals for observations at 13:45 local time (Korea Standard Time).

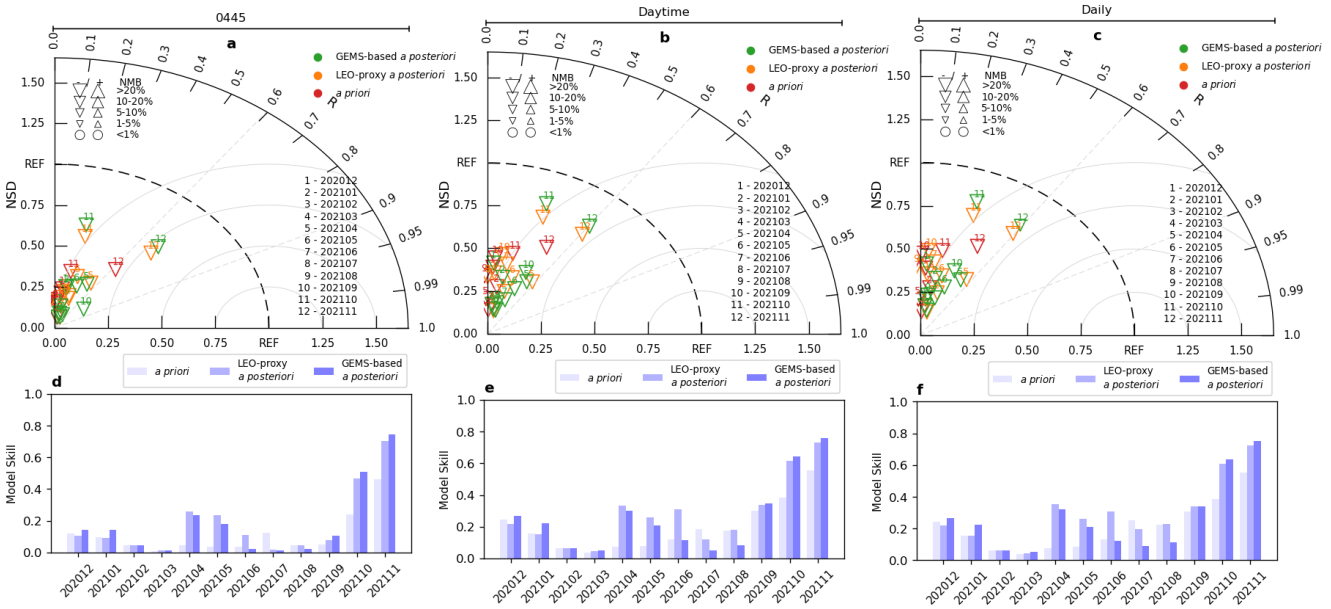

Figure S5. Same as Figure 3 but for columnar NO_2 measurements from the Pandonia Global Network (PGN).

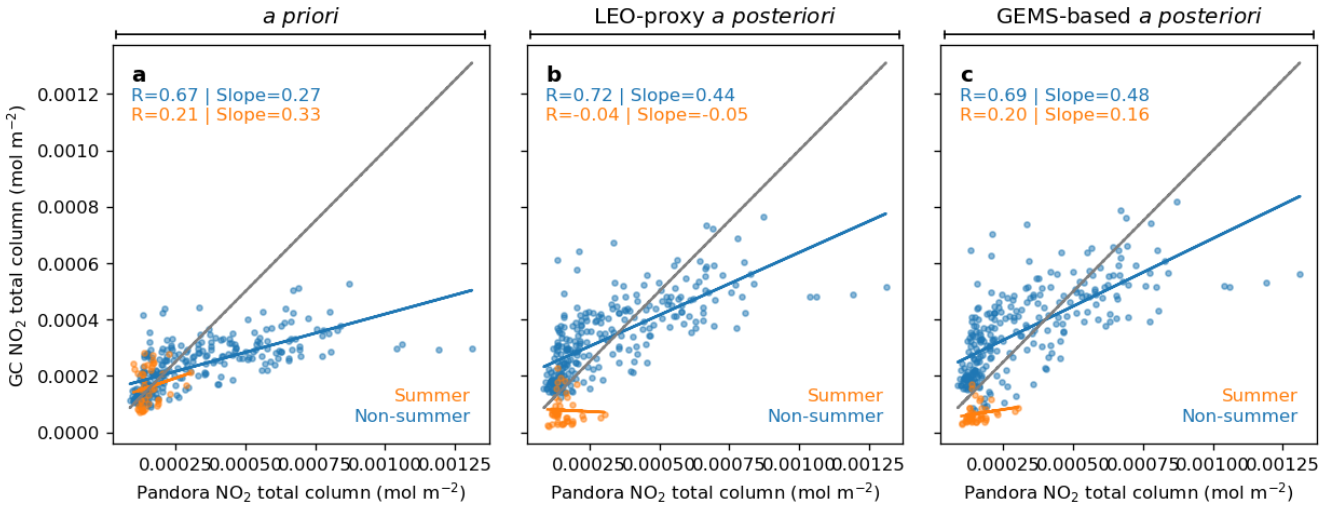

Figure S6. Scatter plots between modelled and observed columnar NO_2 from the Pandonia Global Network (PGN) at the Beijing-RADI site. The modelled columnar NO_2 is driven by *a priori* (**a**) and *a posteriori* NO_x emissions from both the "LEO–proxy" (**b**) and "GEMS–based" (**c**) inversions. The points distinguish between summer (orange) and non–summer (blue) months. The linear correlation coefficients (R) and linear regression slopes between the modelled and observed columnar NO_2 are also shown for each case.

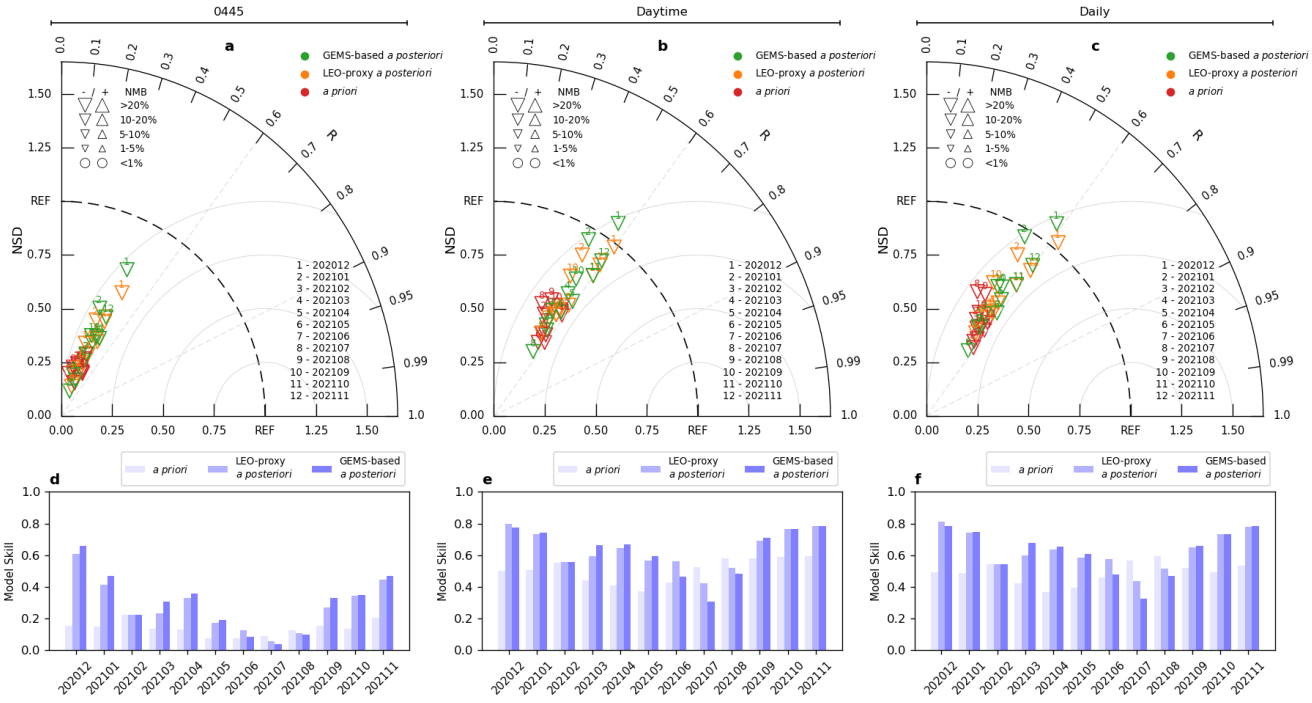

Figure S7. Same as Figure 3 but for surface NO_2 measurements from the China National Environmental Monitoring Centre (CNEMC).

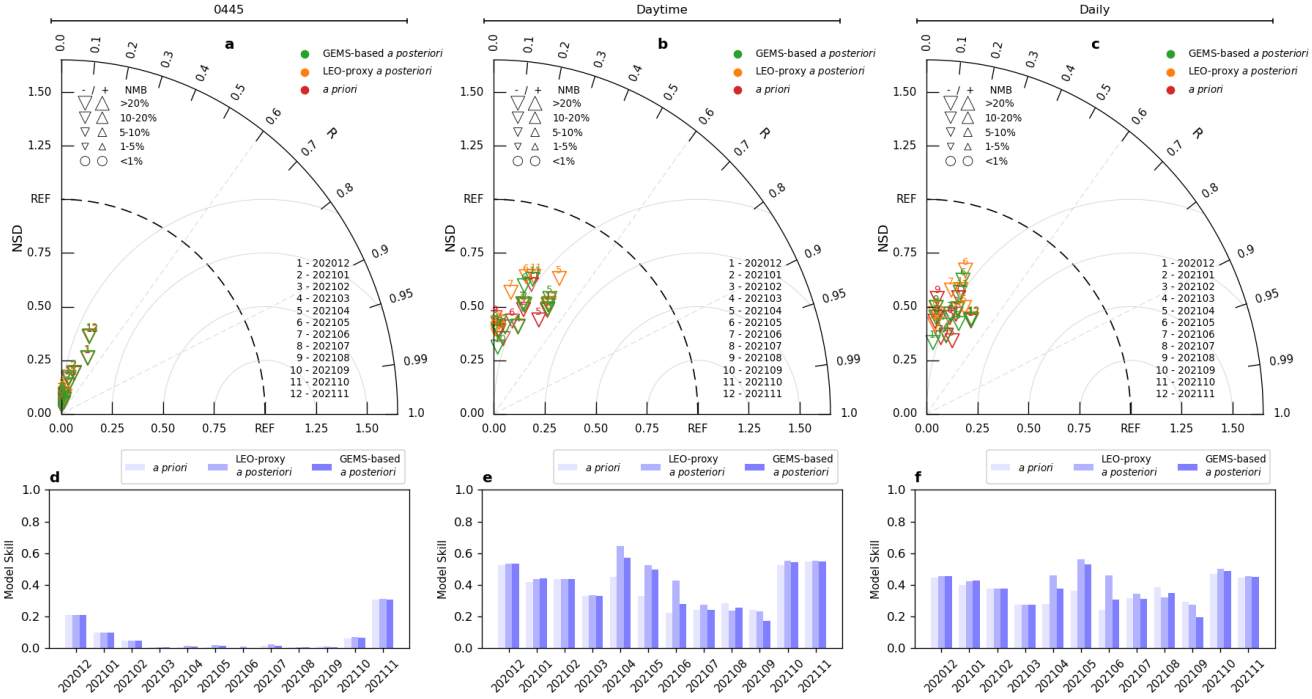

Figure S8. Same as Figure 3 but for surface NO_2 measurements from the Central Pollution Control Board (CPCB) of India.

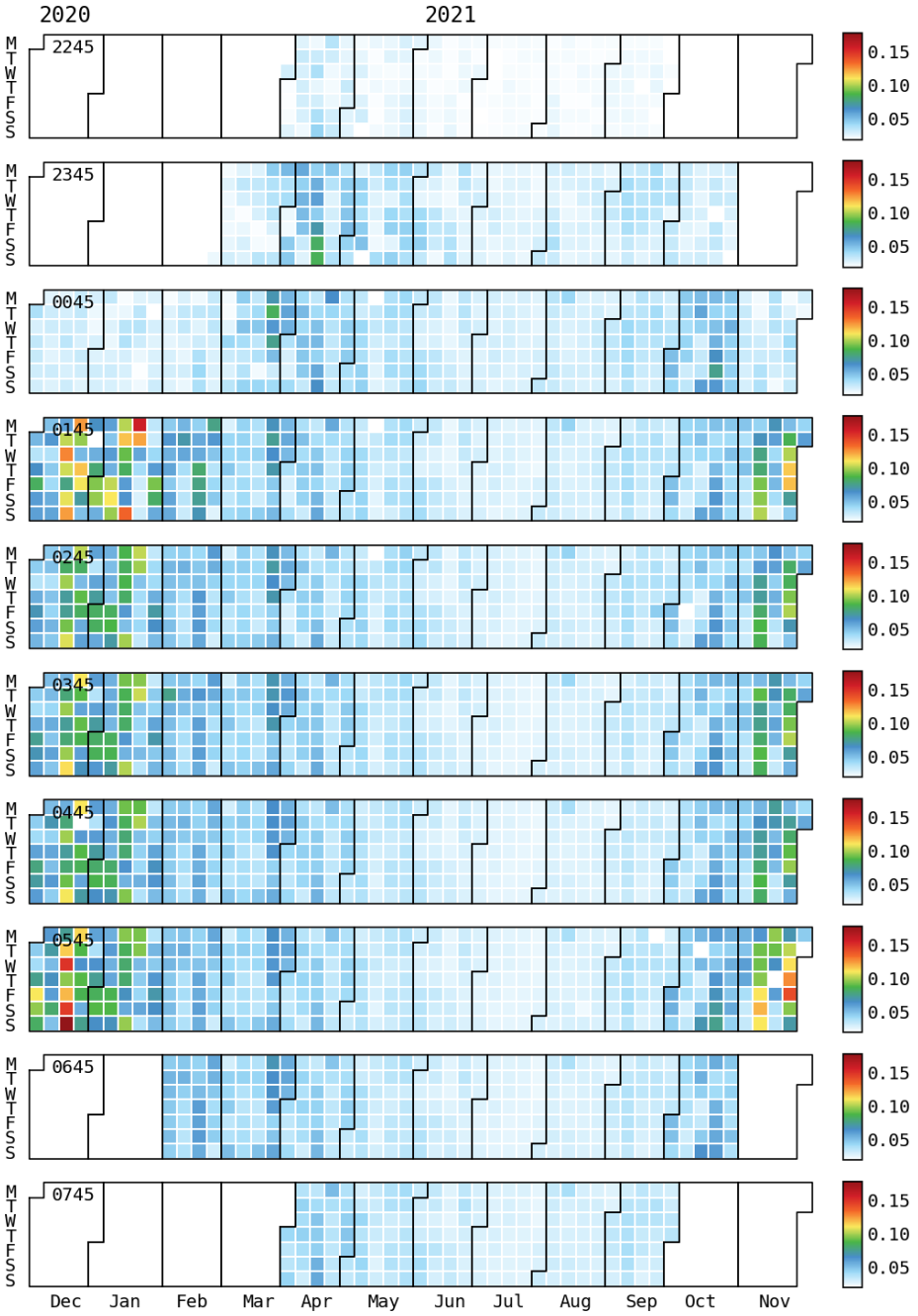

Figure S9. Hourly distributions of GEMS tropospheric NO_2 retrievals averages for all observations over the pan–Asian region.

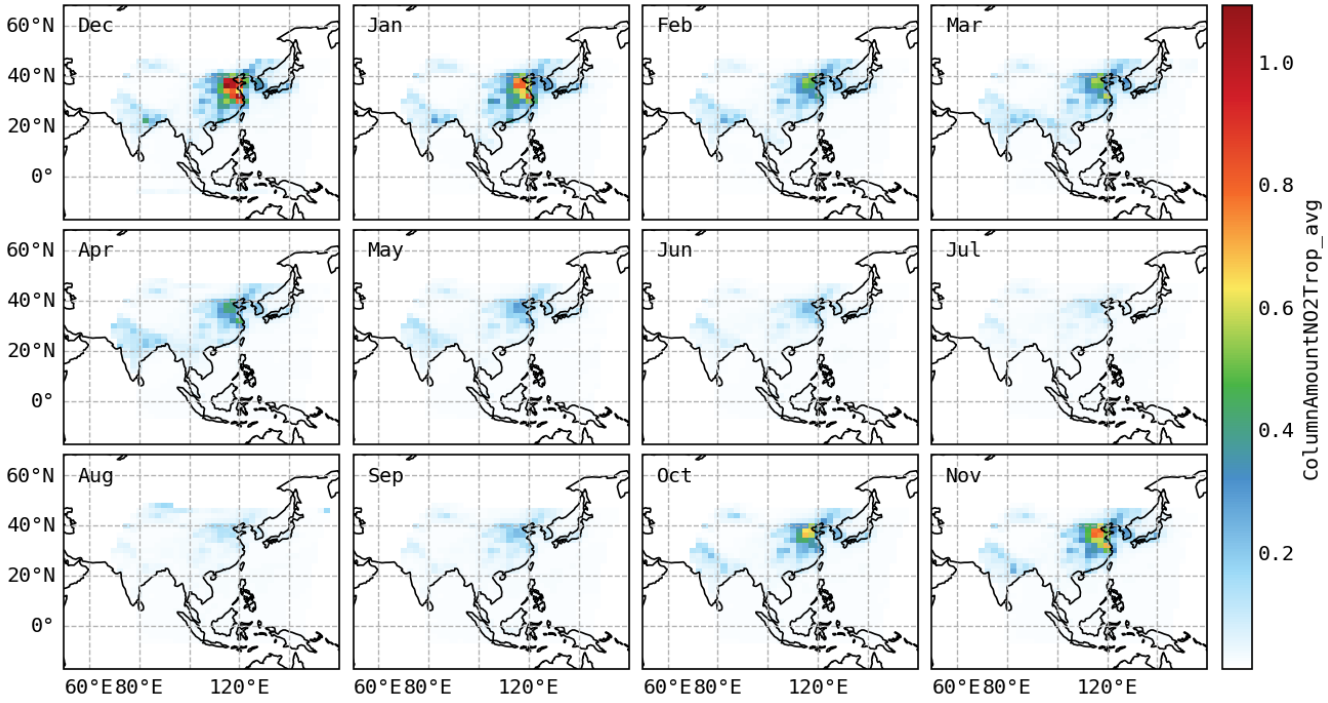

Figure S10. Geographical distributions of monthly averages of GEMS tropospheric NO_2 retrievals for all daytime observations.

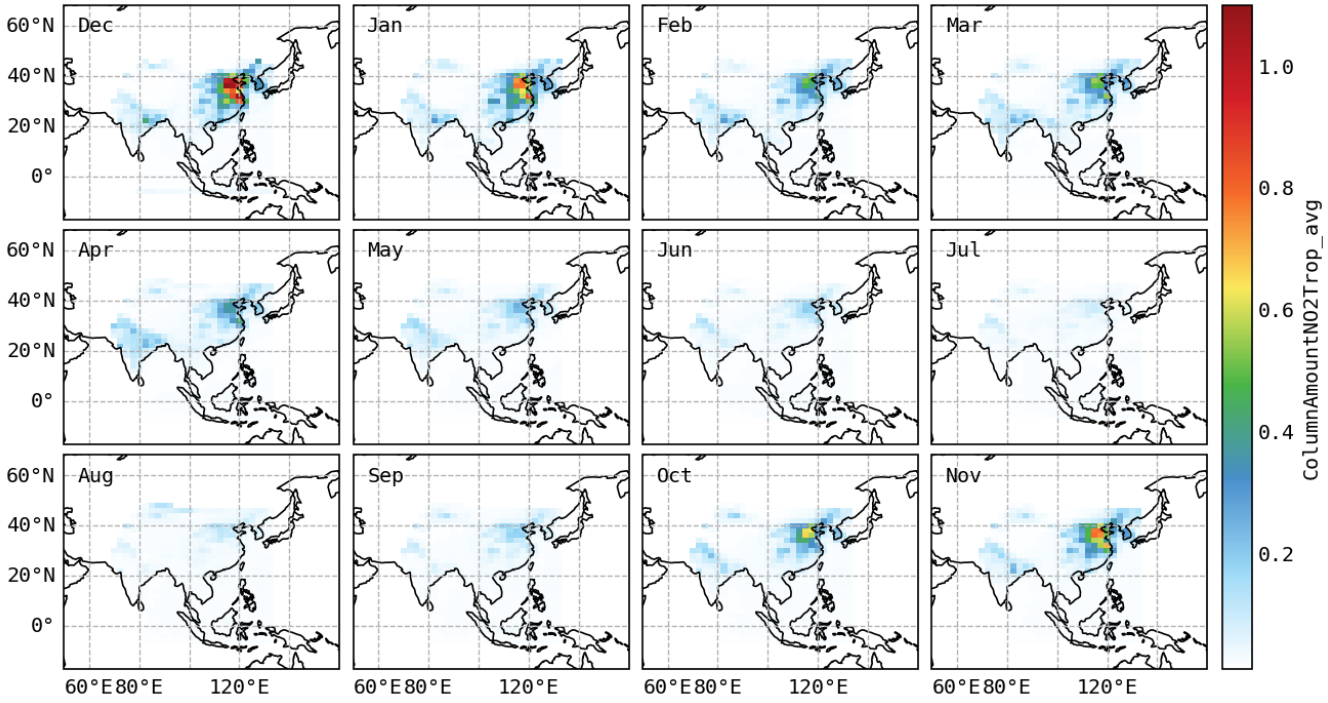

Figure S11. Geographical distributions of monthly averages of GEMS tropospheric NO_2 retrievals for observations at 13:45 local time (Korea Standard Time).

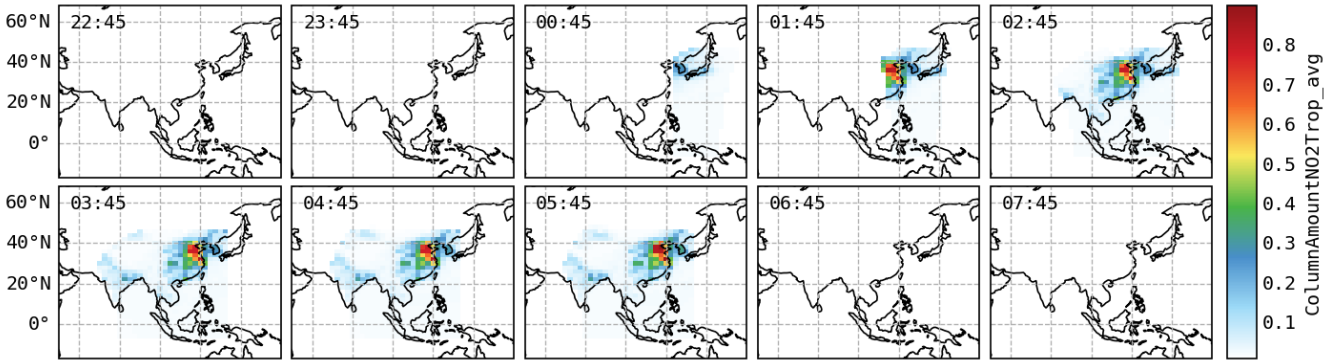

Figure S12. Diurnal variability of GEMS tropospheric NO_2 retrievals for January 2021.

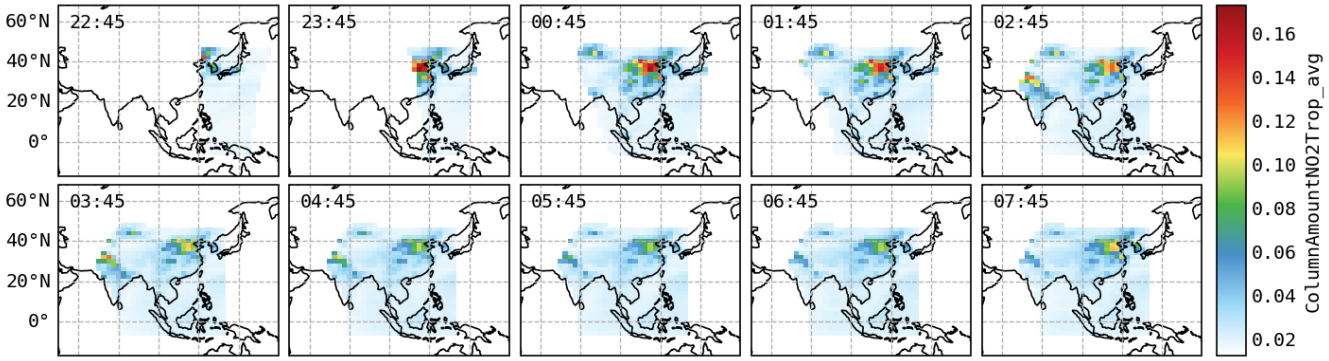

Figure S13. Diurnal variability of GEMS tropospheric NO_2 retrievals for July 2021.

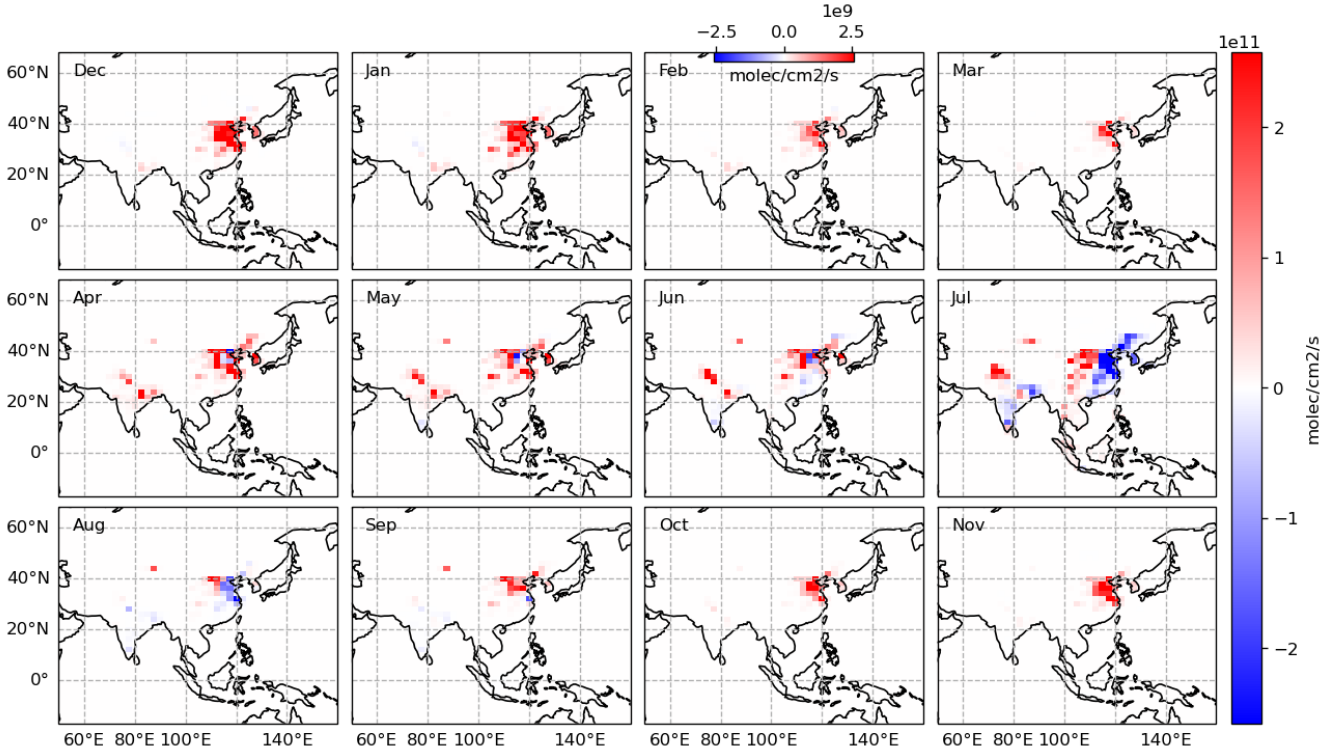

Figure S14. Geographical distributions of the differences between the "LEO–proxy" *a posteriori* and *a priori* anthropogenic NO_x emissions. Note that the differences in February are relatively small; therefore, a different color scale is used to highlight the spatial patterns.

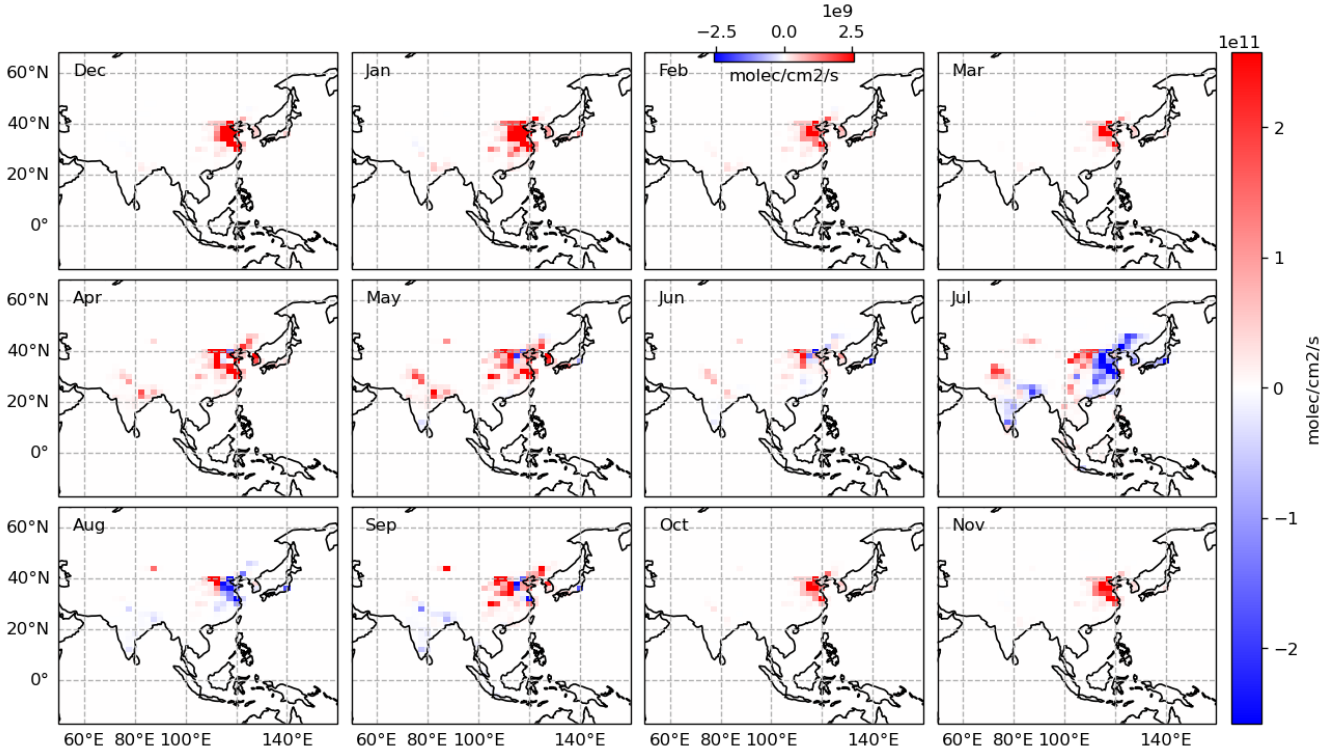

Figure S15. Geographical distributions of the differences between the "GEMS–based" *a posteriori* and *a priori* anthropogenic NO_x emissions. Note that the differences in February are relatively small; therefore, a different color scale is used to highlight the spatial patterns.

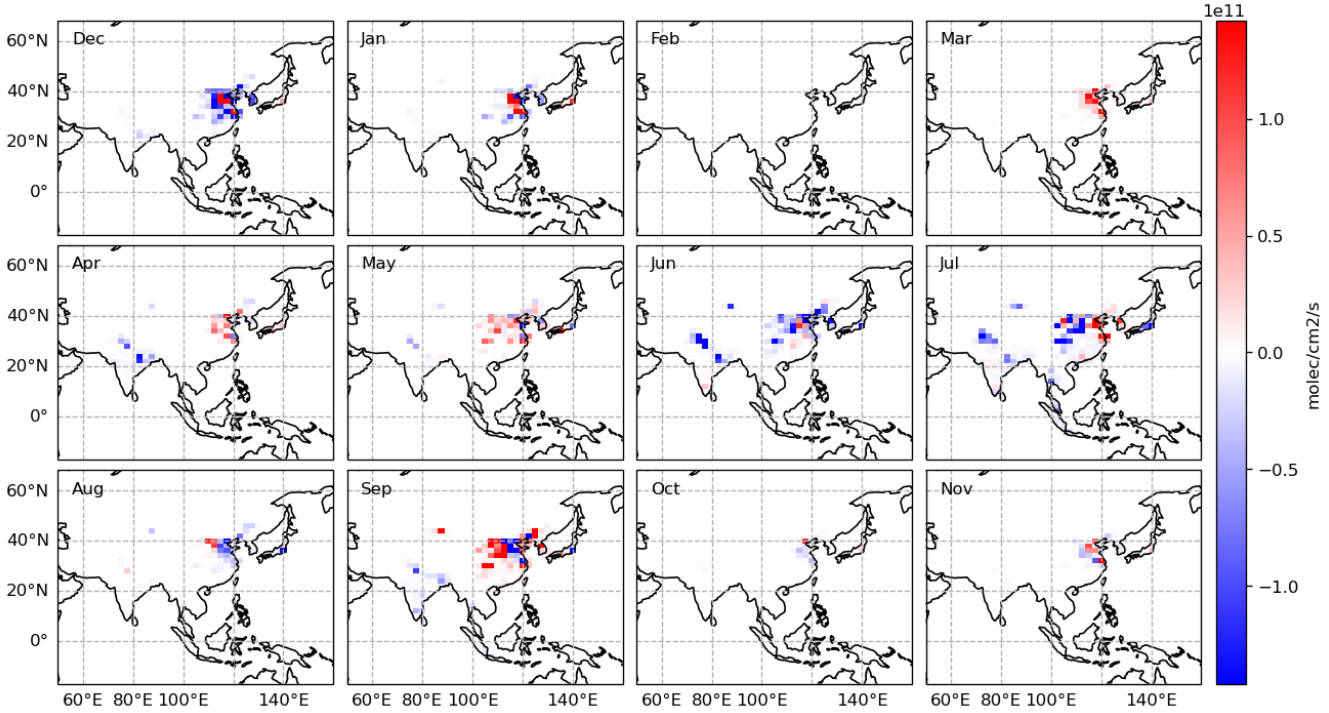

Figure S16. Geographical distributions of the differences between the "GEMS–based" and "LEO–proxy" *a posteriori* anthropogenic NO_x emissions.

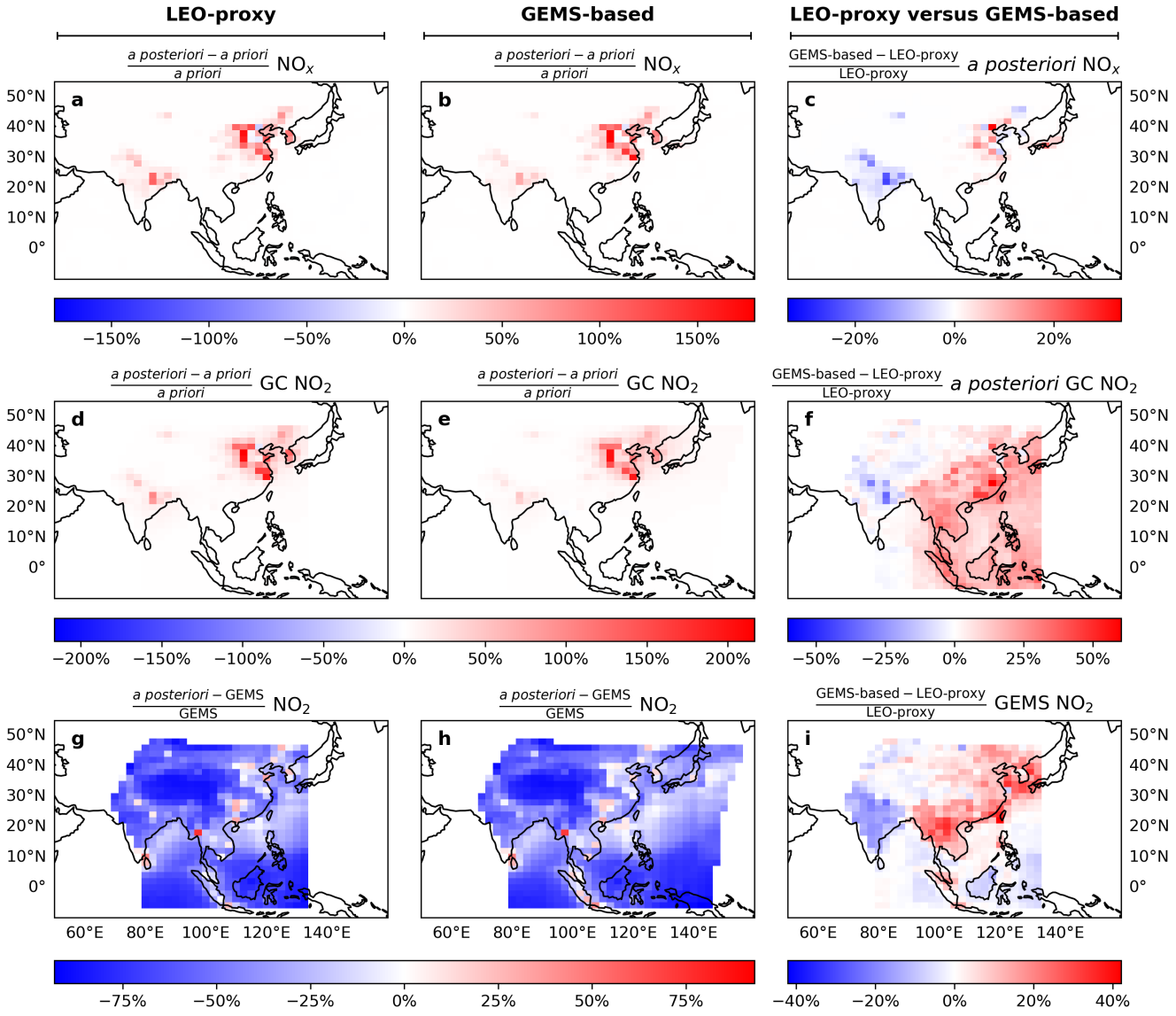

Figure S17. Results for April 2021 from the "LEO–proxy" and "GEMS–based" inversions, along with a comparison between them. Panels **a-i** specifically show percentage values corresponding to panels **a3, b3, c1, a9, b9, c3, a8, b8, c2** in Figure 4.

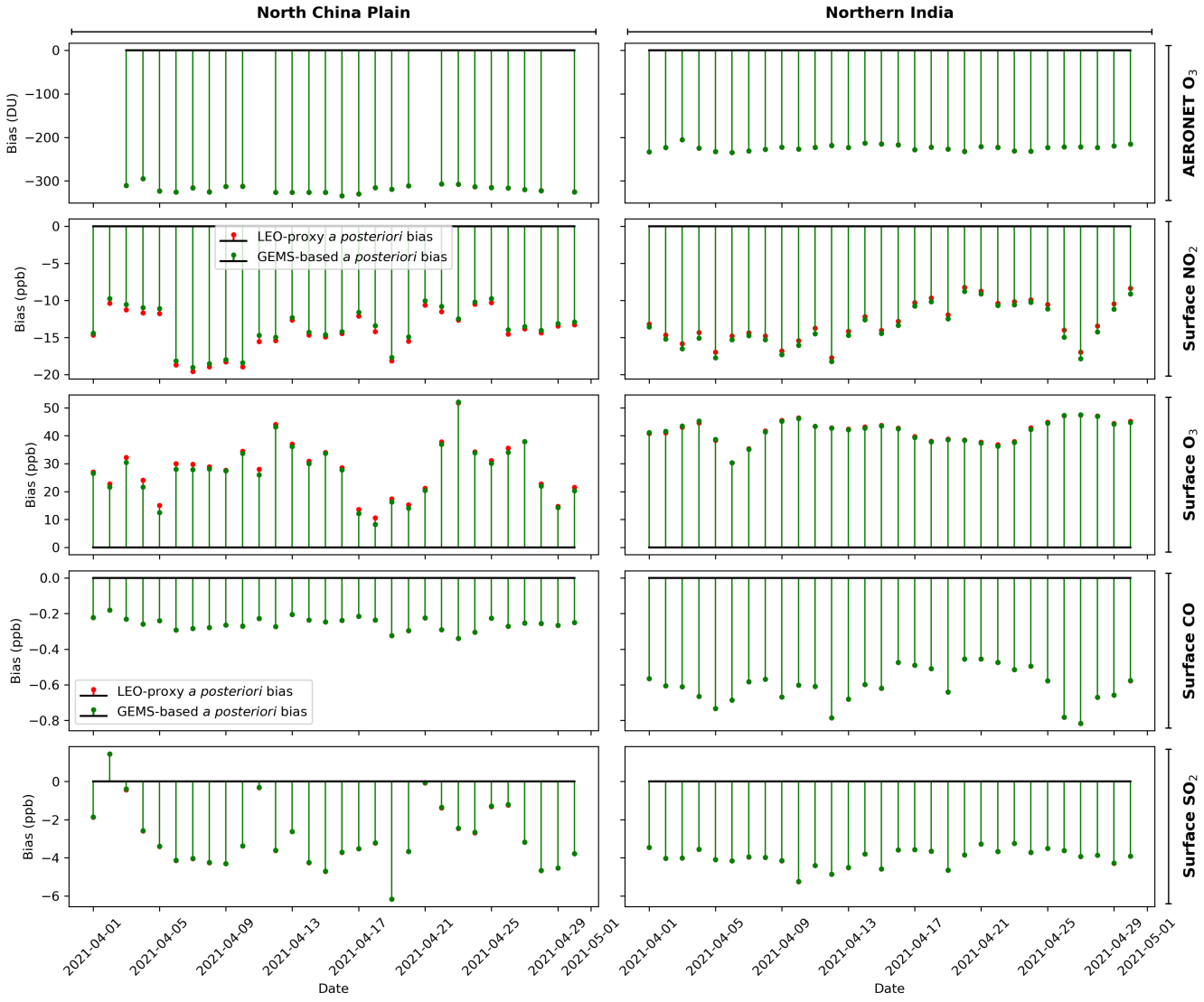

Figure S18. Stem plot of model–observation bias in columnar O_3, surface NO_2, surface O_3, surface CO, and surface SO_2 over the North China Plain and Northern India subregions in April 2021.

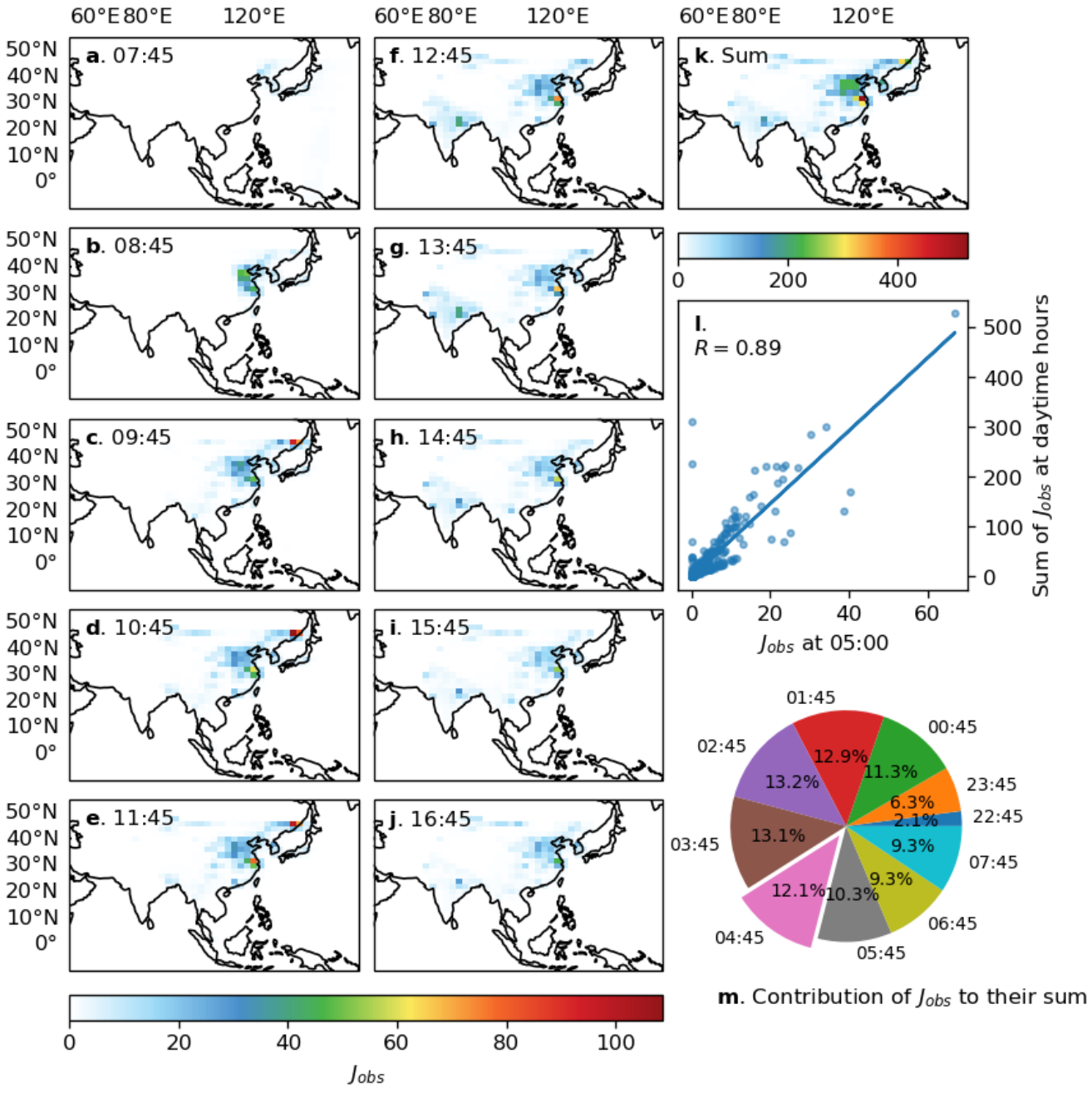

Figure S19. Geographical distributions of the observational part of the cost function (J_{obs}) at 07:45 (**a**), 08:45 (**b**), 09:45 (**c**), 10:45 (**d**), 11:45 (**e**), 12:45 (**f**), 13:45 (**g**), 14:45 (**h**), 15:45 (**i**), and 16:45 (**j**) local time (Korea Standard Time) for April 2021. Panel **k** shows the sum of J_{obs} across all hours. Panel **l** shows the scatter plot between the sum of J_{obs} across all hours and the J_{obs} at 13:45 local time, with the Pearson correlation coefficient (R) annotated. Panel **m** shows the contributions of J_{obs} at different hours to the total J_{obs} across all hours.